Bio-Design and Manufacturing (2018) 1:254–264
https://doi.org/10.1007/s42242-018-0027-9

RESEARCH ARTICLE

Origami meets electrospinning: a new strategy for 3D nanofiber scaffolds

Juqing Song[1,2] · Guanglin Zhu[1] · Huichang Gao[1,3] · Lin Wang[1,3] · Nanying Li[1] · Xuetao Shi[2] · Yingjun Wang[1,2]

Received: 19 September 2018 / Accepted: 30 October 2018 / Published online: 20 November 2018

Abstract

Inspired by the constitution of things in the natural world, three-dimensional (3D) nanofiber scaffold/cells complex was constructed via the combination of electrospinning technology and origami techniques. The nanofiber boxes prepared by origami provided a limited space for the layer-by-layer nanofiber films, and the human fetal osteoblasts (hFOBs) seeded on the both sides of the nanofiber films were expected to facilitate the bonding of the adjacent nanofiber films through the secretion of extracellular matrix. Specifically, the hFOBs presented 3D distribution in the nanofiber scaffold, and they can stretch across the gaps between the adjacent nanofiber films, forming the cell layers and filling the whole 3D nanofiber scaffold. Eventually, a 3D block composed of electrospun nanofiber scaffold and cells was obtained, which possesses potential applications in bone tissue engineering. Interestingly, we also created 3D nanofiber structures that range from simple forms to intricate architectures via origami, indicating that the combination of electrospinning technology and origami techniques is a feasible method for the 3D construction of tissue engineering scaffolds.

Keywords Electrospinning · Origami · 3D construction · Nanofiber scaffold/cells complex

Introduction

Electrospinning, as a universal and cost-effective technology, has aroused worldwide attention and has been explored for extensive applications including photovoltaic devices [1], actuators [2, 3], filtration, catalyst supports [4], dielectric separators [5–8], drug delivery [9–12], composite reinforcements [13–15]. In recent years, electrospinning has been widely adopted in tissue engineering because it can continuously produce nano- to microscale fibers that simulate the structure of extracellular matrix (ECM) [16–19]. Although electrospun nanofibers possess many merits including large surface area-to-volume ratio, high specific surface and multiple designs of surface modification [20–22], traditional electrospinning only can prepare two-dimensional (2D) membranes due to the technical limitations. To overcome the inherent nature of the electrospinning process and obtained three-dimensional (3D) structures, two main kinds of methodologies have been developed to address this issue [23]. The first one relies on the precise manipulation of the electrospinning process via either continuous electrospinning or multilayer electrospinning [11, 24, 25], introducing 3D template to replace the 2D planar collector [26–28] or adjusting parameters (such as solution concentration, electric field strength and relative humidity) to realize the self-assembly of nanofibers [29–31]. 3D nanofiber structure with a thickness of several hundred micrometers could be obtained by continuous electrospinning time, but this was time-consuming and the thickness of the 3D structure was still limited [25]. Most researchers designed collectors with micro-/nanoscale layouts to fabricated patterned nanofibers,

Juqing Song and Guanglin Zhu have contributed equally to this work.

Electronic supplementary material The online version of this article (https://doi.org/10.1007/s42242-018-0027-9) contains supplementary material, which is available to authorized users.

✉ Xuetao Shi
shxt@scut.edu.cn

✉ Yingjun Wang
imwangyj@163.com

1 National Engineering Research Centre for Tissue Restoration and Reconstruction, South China University of Technology, Guangzhou 510006, People's Republic of China

2 Department of Biomedical Engineering, School of Materials Science and Engineering, South China University of Technology, Guangzhou 510006, People's Republic of China

3 School of Medicine, South China University of Technology, Guangzhou 510006, People's Republic of China

and they focused on the configuration in microscale, rather than the 3D architecture in macroscale [32–35]. Although 3D cotton-like nanofiber structures were prepared by adjusting electrospinning parameters, the mechanism of the nanofiber assembly was uncertain and the mechanical properties of the 3D structures were poor. Instead of direct control over electrospinning process, the second one realized 3D construction through post-treatment of electrospun nanofibers, such as overlaying, folding and curling [36–38]. Post-treatment is relatively simple, but the 3D nanofiber structures often have large distances between adjacent fiber surfaces, and in this case, cells only adhere and spread on the 2D surfaces rather than forming a bridge between adjacent surfaces. Thus, the 3D nanofiber structures fabricated by post-treatment cannot be directly used for tissue engineering. To improve this methodology, we examined closely the processes of folding and unfolding, that is, origami [39], and proposed a facile and effective method for 3D construction of electrospun nanofibers by combining the origami and electrospinning.

As a traditional paper art, origami can produce elegant and intricate 3D objects from planar sheets through a series of folding techniques [39]. Since people recognized that nature achieved complex architectures ranging from proteins [40] to plants [41] via the utilization of controlled folding and unfolding sequence, the method of origami assembling has attracted significant scientific and technological interest. So far, the novel origami assembly has been used to fabricate DNA-based objects [42, 43], which are nanoscale. In addition, nano- to mesoscale structures also have been obtained via origami, such as 3D metal objects [44–47] and silicon solar cells [48], that are lithographically patterned and spontaneously folded via surface tension effects [49, 50]. Therefore, how to exert the ability to assemble electrospun structures of arbitrary 3D architecture and functionality with the ease and versatility of origami is significant.

Here, we combine electrospinning technology with origami techniques to construct 3D nanofiber scaffold/cells complex and investigated its potential applications for tissue engineering. As shown in Fig. 1, there are two key issues in this method: one is the utilization of the electrospun nanofiber boxes, and the other is the double seeding of human fetal osteoblasts (hFOBs) on the nanofiber films. In our expectation, the nanofiber boxes can provide a limited space for the nanofiber films, while the double seeding of hFOBs can closely bond the adjacent nanofiber films by the secretion of ECM. In addition, we incorporated nanohydroxyapatite (nHA) particles into polycaprolactone (PCL) nanofibers to improve the mechanical properties. Finally, we also created 3D nanofiber structures that range from simple forms to intricate architectures via origami. In one word, the combination of electrospinning technology and origami techniques for the construction of 3D nanofiber scaffold/cells complex is practicable and it provides a new strategy for the tissue engineering.

Materials and methods

Materials

The PCL pellets (molecular weight 80,000), nHA powders (particle size less than 200 nm) and Docusate sodium salt (AOT, BioUltra) were purchased from Sigma-Aldrich (USA). Dichloromethane (DCM, AR) and dimethylformamide (DMF, AR) were purchased from Aladdin (China). All chemical reagents were used as received.

Preparation of PCL/nHA composite nanofibers

A certain quality of nHA (0, 0.156, 0.350 and 0.600 g) and AOT (0.005 g) were simultaneously added to a 10-mL mixture of DCM and DMF (volume ratio = 1:1) and underwent ultrasonic dispersion for 60 min. During ultrasonication, an anionic surfactant AOT was added to promote the complete dispersion of nHA in DCM/DMF and lower the surface tension of the mixed solution [51]. Cold water was then added discontinuously to the ultrasonic cleaner (SB-5200DT, Ningbo Scientz Biotechnology, China) to ensure a constant temperature. After that, the PCL (1.4 g) was added to the homogeneous suspension of nHA/(DCM + DMF) and completely dissolved by continuous magnetic stirring overnight at room temperature (RT) following the pretreatment of stirring (60 min) and ultrasonication (30 min). According to the initial quality of nHA, a series of PCL/nHA compounds with nHA concentrations of 0, 10, 20 and 30 wt% were produced, which were the mass ratios of nHA and the total solute (nHA + PCL) in the final mixtures. Before electrospinning, for each trial, the PCL/nHA mixture was ultrasonicated for 30 min.

The electrospinning was conducted using a conventional procedure as described in our previous work [52]. Typically, the mixture was filled in a 10-mL plastic syringe equipped with a 24-gauge stainless steel blunt-tipped needle (inner diameter: 0.30 mm), and then, electrospinning was performed under a series of constant parameters: flow rate, 1 mL/h; distance between the blunt needle tip and the collector, 12 cm; supplied positive voltage, 16.2 kV; temperature, 37 °C ± 3; and relative humidity, 45% ± 3. All nanofibers were collected with an aluminum foil wrapped on a grounded rotary drum (diameter = 100 mm). The rotating speed of the rotary drum was 200 rpm, and the collecting time was 13 min (for morphological characterization) or 4.5 h (for the other physicochemical characterization and 3D construction via origami). To obtain samples with suitable size and thickness for mechanical characterization and origami, the spinneret

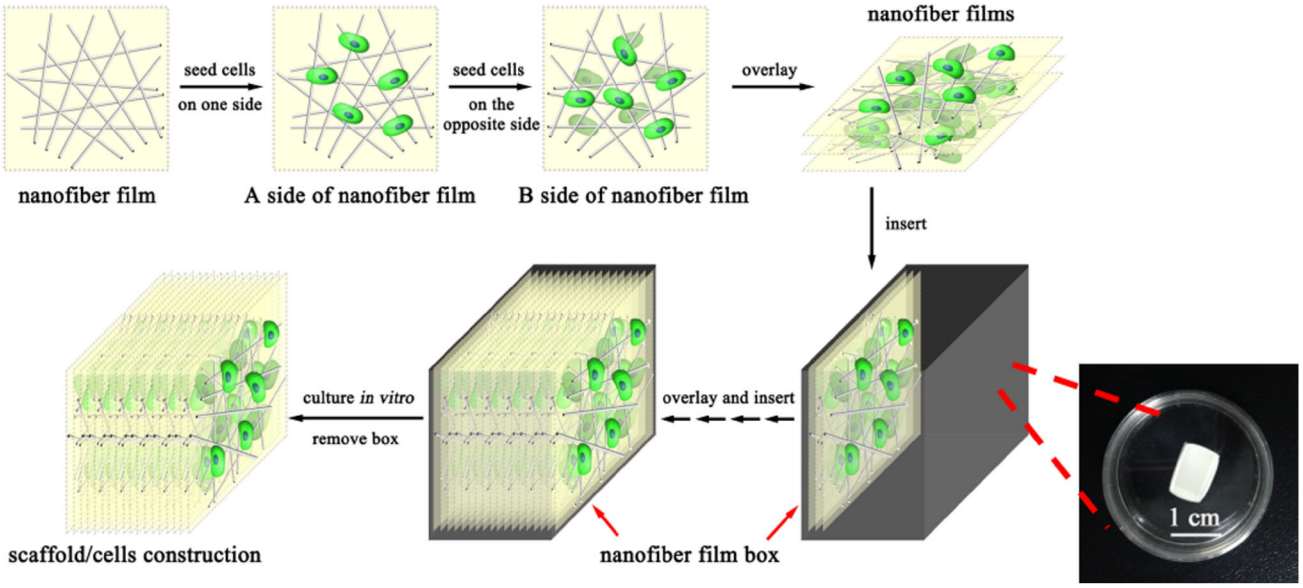

Fig. 1 Illustration of the construction process of the 3D nanofiber scaffold/cells complex. The inset is the nanofiber box prepared by origami

moved along the lateral scanning frame during electrospinning (moving distance, 54 mm; and moving speed, 27 mm/s). The collected nanofiber films were subsequently dried for at least 2 days under vacuum to remove any residual solvents. The electrospinning process was conducted using a commercial electrospinning machine (FM1108-Electrospinning System, Beijing Future Material Sci-tech, China).

To construct 3D nanofiber scaffolds with massive structure, we assembled the electrospun films via origami, and the specific process is as follows (Fig. 1): (1) The PCL/nHA composite nanofiber films were cut into small squares (1.0 cm × 1.0 cm) using a commercial punch; (2) In addition, the nanofiber films were also cut into a plurality of rectangles [width of 2.7 cm (1.0 cm × 2 + 0.7 cm) and length of 3.0 cm (1.0 cm × 3)], which were used for the origami construction of nanofiber boxes (the inset in Fig. 1, without cover, length of 1.0 cm, width of 0.7 cm and height of 1.0 cm); (3) The normal cultured hFOBs were seeded on one side of the nanofiber film (1) with an appropriate concentration ($5 \times 10^4/cm^2$), adhered and cultured for 1 day, a duration that ensure cells adhere to nanofibers well with a suitable density; (4) Turning the nanofiber film (3), seeding hFOBs on the other side of the nanofiber film with the same concentration and culturing for 1 day; (5) When hFOBs adhered well on the both sides of the nanofiber film, the nanofiber films (4) were overlaid layer by layer and inserted into the nanofiber boxes (2). During the process of overlaying, the structural integrity of the nanofiber films should be ensured; (6) Repeating the operation of overlaying and inserting (5) until the nanofiber boxes were filled with nanofiber films; (7) The 3D structures (6) were transferred into a humidified incubator with 5% CO_2 (37 °C) and then cultured in vitro. During the process of the culture, the cell culture medium was refreshed every three days; (8) When endpoints (14 and 30 days) were reached for assays, the 3D structures were removed and detected via various analysis methods. In this process, we expect the hFOBs will proliferate and migrate through the nanofiber films, which are confined in the nanofiber boxes. Most importantly, the cells adhered on the both sides of the nanofiber films also secrete ECM, which can bond the adjacent nanofiber films, resulting in the formation of 3D scaffold/cells complex.

For the nanofiber box, the process of origami construction is shown in Fig. 2: (1) The nanofiber film was cut into rectangles (3.0 cm × 2.7 cm) using a commercial punch; (2) In the length direction, the rectangle was equally divided into three parts and the cuts were 1.0 cm (the red dotted lines); (3) The gray area ⑤ in the middle served as the bottom of the nanofiber box, and the white areas ② and ④ were folded up (which were perpendicular to the bottom); (4) Like the white areas, the blue areas were also fold up as the sides of the nanofiber box; (5) With the folding of the blue areas, the orange areas ① and ③ were folded up and overlapped with the white areas (① was overlapped with ② and ③ was overlapped with ④). It should be noted that the overlapped areas were bonded using the PCL/DCM solution with a concentration of 18% (w/v), which had been used in our previous work [53].

Morphologies of the composite nanofibers and the 3D scaffolds

The micromorphologies of the nanofibers and the 3D scaffolds were observed by a field emission scanning electron microscope (FESEM, Merlin, Zeiss, Germany) with an accel-

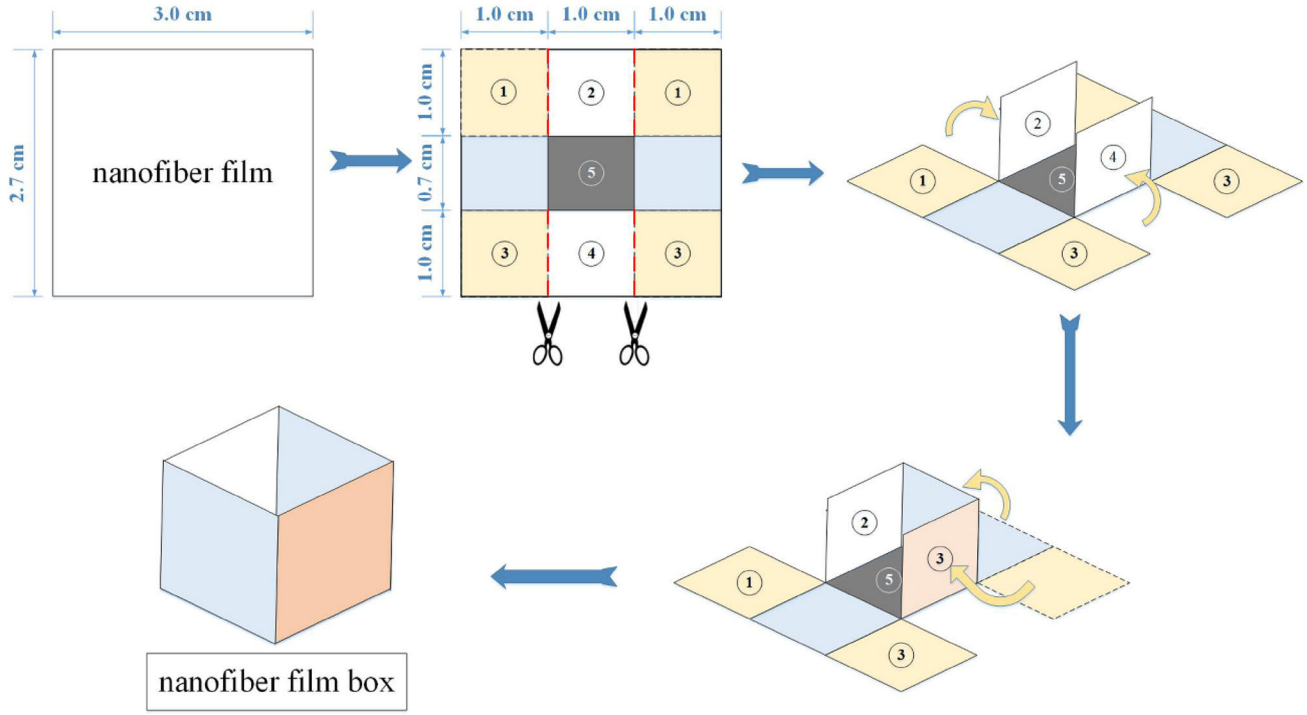

Fig. 2 Process of the origami construction of the nanofiber box. The red dotted lines are the cuts

erating voltage of 5 kV. Prior to SEM imaging, the samples were sputtered with platinum for 120 s by a high-vacuum sputter coater ion sputter (Q150T, Quorum, UK). Moreover, the macromorphologies of the nanofiber boxes and the 3D scaffold/cells complex were characterized via a digital single-lens reflex camera (DSLR, Nikon, Japan).

Mechanical properties of the composite nanofiber films

The mechanical properties of the nanofiber films were determined using a universal material testing machine (5967, Instron, USA) at a crosshead speed of 5 mm/min with a 250-N load cell (the maximum) in an ambient environment. All samples were sectioned into dumb-bell shapes with a test rectangular dimension of 13 × 5 mm (length × width) and a thickness of about 0.08 mm, measured using a digital screw micrometer. At least five samples were tested for each type of nanofiber films, and the mean and standard deviation were calculated.

Surface components of the nanofiber

Powder X-ray diffraction patterns of PCL, nHA and PCL/nHA composite nanofibers were recorded on a X-ray diffractometer (XRD, D8 ADVANCE, Bruker, Germany) with Cu Kα ($\lambda = 0.15418$ nm) incident radiation. The XRD data were collected between 5° and 90° in intervals of 0.02° and a scan rate of 2°/min.

Thermal properties of the scaffold

A differential scanning calorimeter (DSC, Pyris Diamond DSC, PerkinElmer, USA) was used in a temperature range of −40 to 100 °C at a heating rate of 5 °C/min under a nitrogen atmosphere to evaluate the thermal properties of the scaffolds. To eliminate the thermal history, all specimens underwent two heat cycles from −40 to 100 °C. Dried samples with a weight of approximately 10 mg were loaded in an aluminum crucible. The thermal stability of the scaffolds was determined using a simultaneous thermal analyzer (STA, STA449 C, Netzsch, Germany) under a nitrogen atmosphere. The temperature range used was 30–1000 °C, with unchanged sample weight and heating rate.

Cell culture

Human fetal osteoblasts (hFOBs, ATCC, USA) were propagated in conventional growth medium, consisting of Dulbecco's modified Eagle's medium (DMEM/F12 (1:1), Gibco, USA), 10% fetal bovine serum (FBS, Gibco, USA) and 1% penicillin/streptomycin stock solution (Beyotime Institute of Biotechnology, China). Studies on cell behaviors were performed with hFOBs within four to five passages, which were digested and collected by the addition of 0.25%

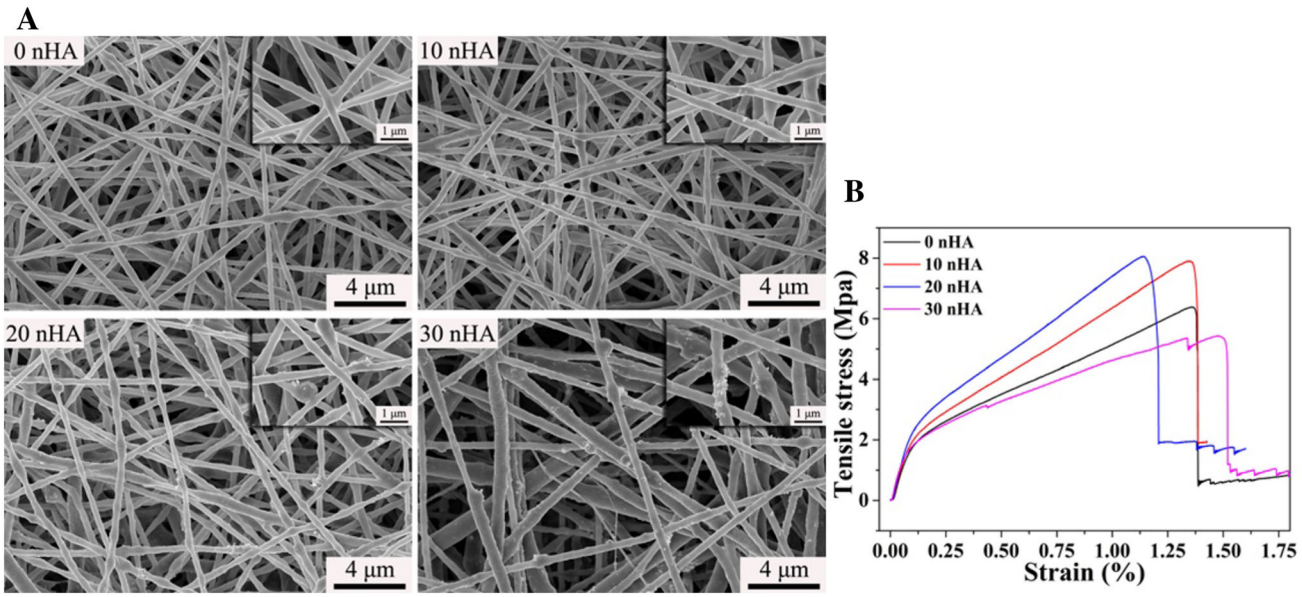

Fig. 3 **a** Surface morphological images of PCL/nHA composite nanofibers with different nHA concentrations (wt%) by SEM and **b** typical tensile stress–strain curves of PCL/nHA composite nanofiber scaffolds with different nHA concentrations (wt%)

trypsin–EDTA solution (Gibco, USA). In all experiments, the cell culture medium was refreshed every 3 days. The PCL/nHA-20 wt% composite nanofiber films which have been sectioned were introduced into 6-well TCP plates (Jet Bio Filtration, China) and sterilized with an irradiation of 15 kGy. After immersing in the cell culture medium for 3 days to remove any residual, the hFOBs were seeded on the nanofiber films as introduced in the chapter of 2.2 (the construction of 3D nanofiber scaffolds with massive structure, Fig. 1).

Assembling of 3D scaffold/cells complex

To analyze the cell behaviors on the 3D nanofiber scaffolds and the assembling of 3D scaffold/cells complex, the staining of cell skeleton/nucleus was performed. The hFOBs were seeded onto the nanofiber scaffolds and cultured for 14 and 30 days. Then, the scaffold/cells samples were transferred to a new TCP plate and washed twice with DPBS. The samples were fixed with 4% neutral formaldehyde (ACS, Aladdin) at 37 °C for 40 min and then immersed in 0.1% Triton X-100 (Biochemical, Aladdin) for 7 min to increase permeability. Finally, the fixed cells were stained with Cell Navigator TM F-Actin Labeling Kit (AAT Bioquest Inc, USA) and DAPI (Beyotime Institute of Biotechnology, China) working solution at 37 °C for 70 and 9 min, respectively. All the stained cells were rinsed thrice and observed by a laser scanning confocal microscope (LSCM, Leica, Germany).

Results and discussion

Morphologies of the composite nanofibers

Considering the application of 3D electrospun nanofiber scaffolds assembled by origami, we incorporate nHA particles to PCL polymer matrix via electrospinning. SEM was used to characterize the surface morphology of the electrospun nanofibers with different nHA concentrations (0, 10, 20 and 30 wt%) under the same conditions, and the results are shown in Fig. 3a. It can be found that the morphologies of PCL/nHA composite nanofibers were similar to that of pure PCL, that is, the nanofibers were randomly oriented, and made up the scaffolds with 3D interconnected pores. Although the pure PCL nanofibers possessed smooth surface and uniform diameter, the intersection of two individual nanofibers slightly fused. Due to the incorporation of nHA particles, the surface of PCL/nHA composite nanofibers became rough, and the distribution of nanofiber diameter was no longer uniform. With the increase in nHA content, this phenomenon became more and more obvious, even when the nHA content was 30 wt%, the composite nanofibers appeared very fine wire drawing. Besides, the size of the individual nanofiber was also not uniform, with the appearance of thick or thin sections and obvious protuberances. This can be explained by the nanoscale effect of nHA, that is, nHA particles are likely to aggregate when present in large quantities. This may lead to the division of the electrospinning solution into two different regions: nHA-rich and nHA-scarce, which reduces the spin ability of polymer solution and the stability of liquid jet during the electrospinning process, resulting in

the nonuniformity of the diameter distribution and the individual nanofiber [52]. Precisely, the content of nHA would be a crucial factor to determine the morphology of the PCL/nHA composite nanofibers.

Mechanical properties of the composite nanofiber films

In addition to the biocompatibility, biodegradability and interconnected pores, the ideal scaffold should also have mechanical stability. The combination of chemical and mechanical properties of scaffold plays an important role in cell proliferation and tissue formation, and it is also a key technique for the successful construction of nanofiber scaffold. The mechanical properties of electrospun nanofiber scaffold include elastic modulus, tensile strength and elongation, which are reflected in the stress–strain curves. Specifically, they correspond to the linear slope of the initial elastic region, the highest point of the coordinate, and the abscissa value corresponding to the highest point of the coordinate, respectively. As shown in Fig. 3b, all the nanofiber scaffolds have similar stress–strain curves, showing the initial elastic region and the final fracture failure. The elastic modulus and tensile strength of PCL/nHA composite nanofiber scaffolds increased significantly with the increase in nHA content. On the contrary, the elongation at break decreased dramatically. When the nHA content increased to 30 wt%, the elastic modulus and tensile strength of the composite nanofiber scaffold decreased, even lower than those of the pure PCL nanofiber scaffold. Interestingly, the stress–strain curve of the PCL/nHA-30 wt% composite nanofiber scaffold showed the double yielding. This may be due to the content of nHA particles is too high, and the nHA aggregates with large scale will break the entanglement of PCL polymer chain, which reduces the mechanical properties of the composite nanofibers, whereas the friction and the slide between the inorganic particle aggregates and organic polymer chain lead to the double yielding after the fracture. In other words, with the appropriate incorporation of the nHA, the elastic modulus and tensile strength of PCL/nHA increased, while the elongation decreased.

For the composite nanofiber scaffolds, the increase in tensile strength may be attributed to the effective integration of nHA and PCL, which is inspired by the organic/inorganic composite nanostructure of natural tissues (such as bone). Higher elastic modulus of elasticity and lower elongation at break can be explained by the fact that the nHA particles endow the polymer nanofibers more hardness and less plasticity during the deformation process, which is the necessary form of the inorganic phase filling. It is well known that nHA can promote the interaction between materials and osteoblasts, improving the bone conductivity. However, the brittleness of nHA has limited its applications, and it is only used in unloaded and nonbearing applications or as the coating material for metal implants [54, 55]. Although PCL is a synthetic polymer material with superior extension performance, it cannot be used in hard tissue engineering because of its poor mechanical properties [56]. Therefore, the combination of the advantages of these two components in composite nanofibers may synergistically overcome their mechanical defects, providing satisfactory nanofiber scaffolds for the application of bone tissue engineering.

Surface components of the nanofibers

XRD was used to analyze the phase composition of pure PCL, nHA and PCL/nHA composite nanofibers, and the results are shown in Fig. 4. It is clear that the main characteristic diffraction peaks of the orthorhombic PCL (semicrystalline polymer) appeared at the positions of 21.26°, 21.86° and 23.54° (2θ) [57], which are corresponding to the (110), (111) and (200) crystal plane of PCL [58], while the independent diffraction peaks of nHA particles appeared at the positions of 31.66°, 32.79° and 33.94° (2θ), which are corresponding to the (211), (112) and (300) crystal plane of nHA [59]. In addition, there were some weak crystallization peaks appeared in the spectrum of nHA, such as the positions of 25.76° (002), 46.56° (222) and 49.35° (213), which are consistent with the positions of standard diffraction peaks of nHA (JCPDS 9-432) [59]. When the inorganic nHA particles were incorporated into PCL polymer matrix, the crystallization peaks of the two components still existed. Namely, the spectra of PCL/nHA composite nanofibers appeared not only the characteristic peaks of PCL, but also the obvious diffraction peaks of nHA, including three independent peaks and three weak diffraction peaks (marked by the green dashed box and dotted lines). It is worth noting that, compared with the pure nHA particles, the crystallization peaks of the nHA incorporated in the composite nanofiber became wider, and the strength decreased significantly, indicating that the nHA

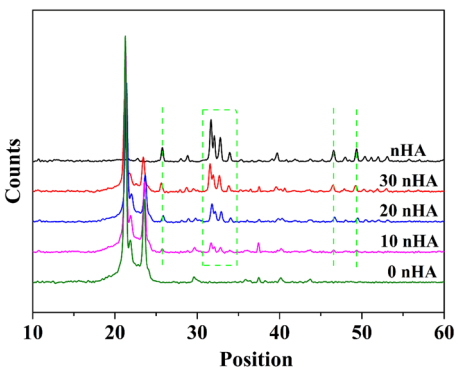

Fig. 4 Crystallinity analysis of nHA powder and PCL/nHA composite nanofiber scaffolds with different nHA concentrations (wt%)

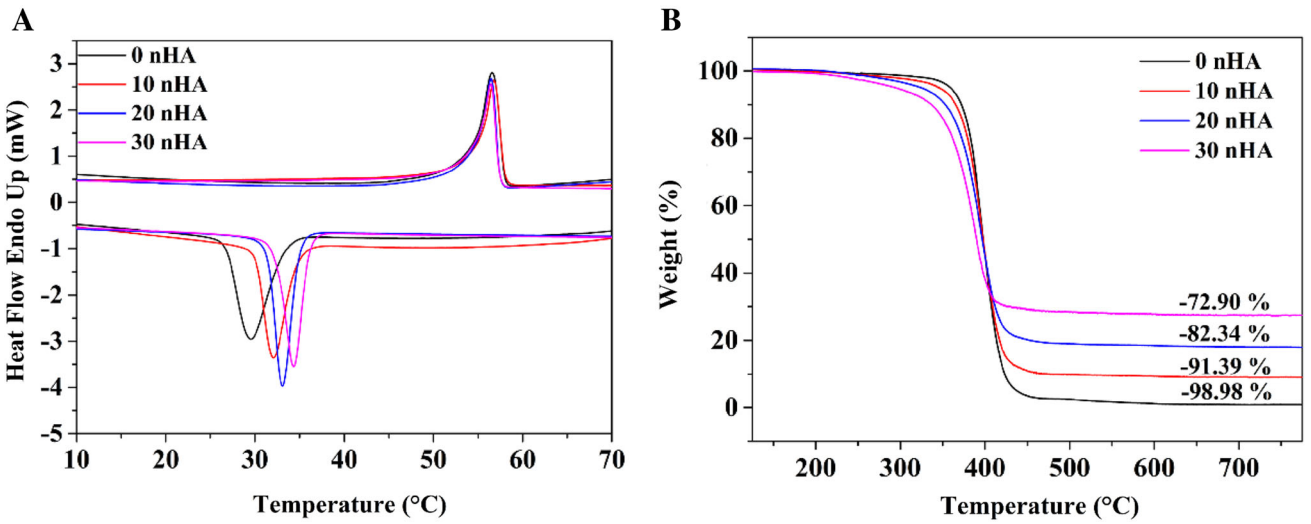

Fig. 5 Variation in the thermal properties of PCL/nHA composite scaffolds with different nHA concentrations (wt%): **a** DSC profiles and **b** TGA profiles

possessed lower crystallinity and smaller grain size. For the PCL/nHA composite nanofibers, with the increase in nHA content, the diffraction peak width of nHA decreased, and the intensity gradually increased. On the contrary, the diffraction peak intensity of PCL gradually weakened, indicating that inorganic nHA not only successfully incorporated into PCL nanofibers, but also interacted with organic PCL polymer matrix. These interactions affected the crystallinity of PCL/nHA composite nanofibers and improved the thermal and mechanical properties.

Thermal properties of the scaffolds

DSC assays were conducted to study the effects of nHA on the crystallization behavior of the PCL polymer matrix. As shown in Fig. 5a, the crystallization temperature (T_c) and melting point (T_m) were determined as the peak temperatures of the first cooling scan curve and the second heating scan curve, respectively. The T_c of PCL/nHA composite nanofibers slightly increased with the increasing content of nHA particles, while the T_m did not significantly change. The increase in T_c may mean that the dispersed nHA particles acted not only as efficient nucleating seeds, but also as barriers to the formation of large crystallites. From Table 1, it is clear that the ΔH_m of the PCL/nHA composite nanofiber scaffolds significantly decreased with the increase in nHA content, indicating that the crystallinity of composite nanofibers decreased. All these slight changes could be attributed to the interactions between the nHA particles and PCL polymer chains, which reduced the chain flexibility and hindered crystallization process [60]. Figure 5b shows the thermogravimetric analysis (TGA) profiles of different nanofiber scaffolds. It is evident that the TGA traces of all nanofiber scaffolds were stable without significant weight loss up to 220 °C. For pure PCL, the initial and maximum weight loss degradation temperatures were 340 °C and 460 °C, respectively. With the increase in nHA content, the initial weight loss degradation temperatures of PCL/nHA composite nanofiber scaffolds significantly decreased, and the maximum weight loss degradation temperatures hardly changed. In addition, the nHA content calculated from the residual after thermal decomposition was slightly lower than that in the initial electrospinning solution, which was 8.61% (10-wt% nHA), 17.66% (20-wt% nHA) and 27.10 (30-wt% nHA), respectively. This is because that the electrospinning time of each sample was about 3.5 h and the precipitation of nHA particles made the homogeneity of the PCL/nHA solution hardly maintained; therefore, the phase separation is likely to lead to decreased nHA content in the composite nanofibers after thermal decomposition, and this adverse effect became more apparent with the increase in nHA content. It is worth noting that the temperature of the maximum weight loss rate decreased with the increase in nHA content. Above all, the incorporation of inorganic nHA particles decreased the thermal stability of PCL nanofibers. This can be explained by the fact that the thermal decomposition of PCL

Table 1 DSC results of PCL/nHA composite nanofiber scaffolds

nHA concentration (wt%)	0	10	20	30
T_c (°C)	29.50	32.08	33.12	34.36
T_m (°C)	56.59	56.75	56.46	56.42
ΔH_m (J/g)	34.49	30.42	24.27	22.90

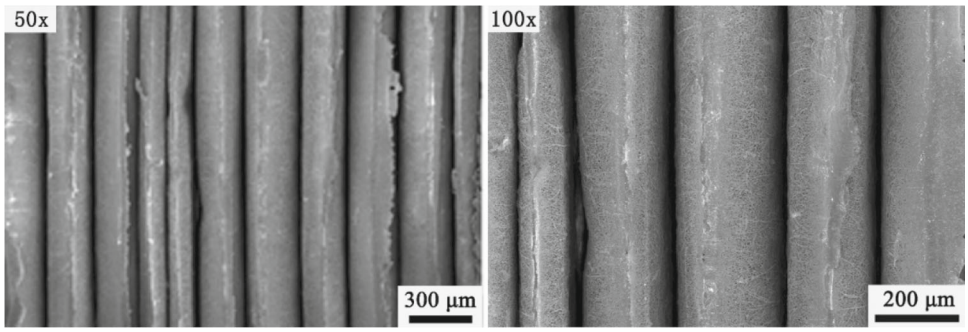

Fig. 6 The microstructure of 3D PCL/nHA composite nanofiber scaffolds via origami

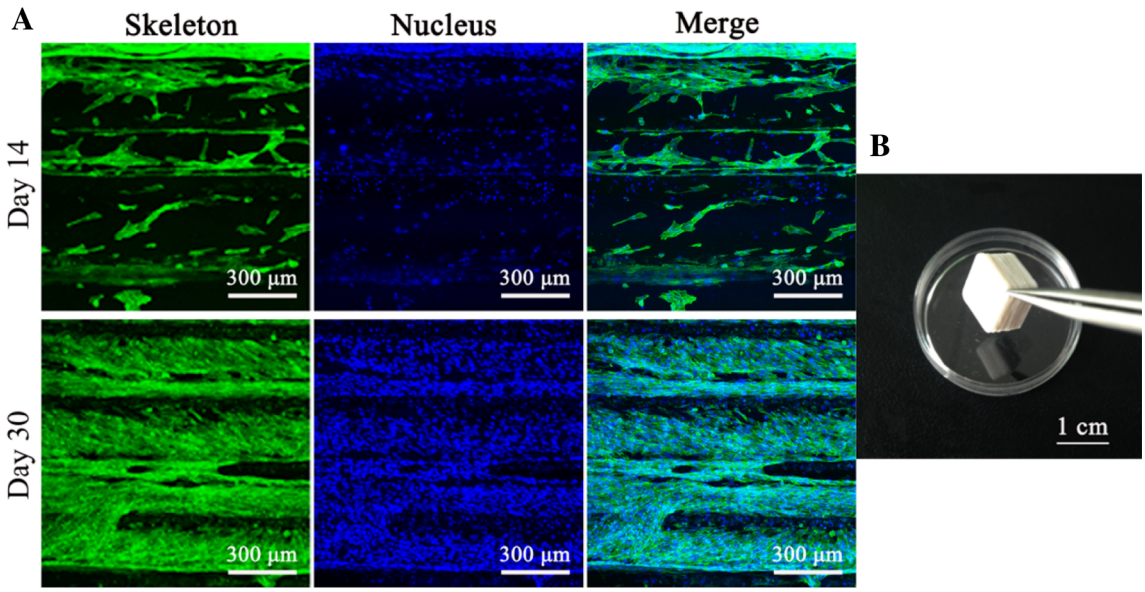

Fig. 7 **a** LSCM images of the distribution of hFOBs on 3D PCL/nHA composite nanofiber scaffolds with 20-wt% nHA after 14 and 30 days of culture and **b** optical photograph of the 3D scaffold/cells complex after 30 days of culture

is divided into two steps [61]: Firstly, the breakage of polymer chains under low temperature leads to the reduced molecular weight of the polymer. Secondly, the terminal of molecular chain was cut into small molecule compounds under high temperature, such as furan, substituted cyclopropane, unsaturated carboxylic acid, whereas the incorporation of inorganic nHA particles may cause the structure feature loss of the PCL polymer molecular chain. Namely, the inorganic particles and organic polymer matrix may combine and interact with each other, such as Van der Waals' force and hydrogen bond. The interactions between the organic and inorganic phases were produced during magnetic stirring, ultrasonic treatment and electrospinning [62].

Morphologies of the 3D nanofiber scaffolds

Considering the results of morphologies (Fig. 3a), mechanical properties (Fig. 3b), surface chemistry (Fig. 4), thermal properties (Fig. 5), we selected PCL/nHA-20 wt% composite nanofibers to construct 3D scaffold via origami. The micromorphology of the 3D composite nanofiber scaffold constructed via origami was characterized by SEM, and the results are shown in Fig. 6. It can be found that each layer of the nanofiber films was independent, and the film thickness was about 200 μm. Importantly, the gap between the adjacent nanofiber films was about 10 μm, which is close to the size of a single cell, allowing cells stretch across the gap, and even contact and adhere on the adjacent nanofiber film. Simultaneously, it is expected to secrete ECM by cells and combine the adjacent nanofiber films by ECM, realizing the construction of 3D nanofiber scaffold/cells complex. In addition, the structure of nanofiber films remained intact after origami, and the morphology of a single fiber was still visible, which are conducive to cell adhesion and growth in nanofiber scaffolds.

Assembling the scaffold/cells complex

The hFOBs on the 3D composite nanofiber scaffold were stained with cell skeleton nucleus and observed by LSCM.

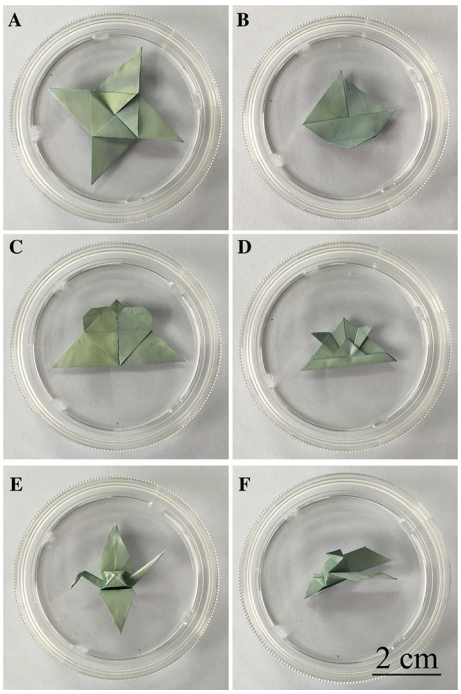

Fig. 8 Optical images of electrospun origami PCL/PANi composite nanofiber structures with simple and intricate shapes. **a–d** Windmill, sailing, heart-shaped bookmark and samurai helmet, and **e–f** crane and peace dove

From Fig. 7a, we can find that hFOBs not only distributed on nanofiber films, but also exist in the gaps of the adjacent fiber films after culture of 14 days, indicating that cells can stretch across the gaps, migrate and adhere on the adjacent nanofiber films. With the prolongation of culture, the cells proliferated, interacted with each other and formed the cell layers after culture of 30 days, which eventually filled and covered the whole 3D nanofiber scaffold. The 3D distribution of hFOBs in the nanofiber scaffold provides the theoretical basis for the filling of the gaps with the ECM and the bonding of the adjacent nanofiber films in the later stage.

After culturing for 30 days, the nanofiber films in the 3D nanofiber box which was prepared by origami were taken out, and the results are shown in Fig. 7b and Video S1. It is clear that the fibrous films were no longer individuals and separate sheets, but a block of nanofiber films. When the nanofiber block was picked by clamping the local part, it would not be scattered and maintained integrity, even with shake. That is, without the use of other bonding process, the nanofiber films limited in a specific space (the nanofiber box prepared by origami) realized the filling of gaps and the bonding of the adjacent nanofiber films through the secretion of ECM, resulting in the formation of the 3D nanofiber scaffold/cells complex.

Macromorphologies of 3D nanofiber structures prepared by origami

To characterize and investigate the origami performance of the electrospun composite nanofibers and the macromorphologies of the 3D structures, the PCL/PANi-1.0 wt% (PANi: polyaniline, green) composite nanofiber, which was collected in the same way with nHA composite nanofiber and held electrical conductivity which is essential for applications in nerve system tissue engineering, was used to construct origami. Different types of origami structures were successfully constructed, as shown in Fig. 8. First, the electrospun PCL/PANi composite nanofiber was tailored into squares (length of 4.2 cm) and then underwent a series of folding and unfolding operations following a basic course. As a result, plenty of 3D structures with simple and intricate shapes were obtained, such as windmill, sailing, heart-shaped bookmark, samurai helmet, crane, peace dove. In the process of origami, the composite nanofiber underwent not only simple operations (folding and unfolding), but also intricate operations (inverted folding, layered folding, valley-shaped folding and mount-shaped folding). Even so, the 3D nanofiber structures obtained by origami had complete shape and enough strength, indicating that the properties of the electrospun composite nanofibers were good enough to construct tailored structure via origami, which is essential for fabricating devices with complex structure.

Conclusions

The 3D nanofiber scaffold/cells complex was obtained through the combination of origami craft and electrospinning technology. Considering the applications of the 3D nanofiber scaffold, the bioactive nHA was incorporated into the biocompatible PCL, and we eventually selected PCL/nHA-20 wt% composite nanofibers to construct 3D scaffolds after investigating the properties of the PCL/nHA composite nanofibers with different nHA concentrations. With the structural design, the layered nanofiber scaffold/cells complex with 3D structure was constructed, and the gap between the layers was about 10 μm. The hFOBs cultured on the both sides of the nanofiber films stretched across the gaps and presented 3D distribution. The ECM secreted by cells realized the gap filling and film bonding between the adjacent nanofiber films, eventually forming a 3D nanofiber scaffold/cells complex. In addition, the origami performance of the electrospun nanofiber was verified by the construction of 3D structures with simple and intricate shapes. These 3D origamis underwent repeated folding and unfolding operations which can maintain the structures and shapes well. All these results indicate the operability of this method—the combination of origami and electrospinning, and it provides

a new strategy for the construction of tissue engineering scaffold.

Supporting information

The verification of the formation of the 3D nanofiber scaffold/cells complex (Video S1).

Acknowledgements This study was financially supported by grants from the National Natural Science Foundation of China (51232002, 51502095, 31771027), the Guangdong Natural Science Funds for Distinguished Young Scholar (2016A030306018) and the Guangdong Natural Science Funds (2017B090911008).

References

1. Onozuka K, Ding B, Tsuge Y, Naka T, Yamazaki M, Sugi S, Ohno S, Yoshikawa M, Shiratori S (2006) Electrospinning processed nanofibrous TiO(2) membranes for photovoltaic applications. Nanotechnology 17(4):1026–1031
2. Jiang S, Liu F, Lerch A, Ionov L, Agarwal S (2015) Unusual and superfast temperature-triggered actuators. Adv Mater 27(33):4865–4870
3. Liu L, Jiang SH, Sun Y, Agarwal S (2016) Giving direction to motion and surface with ultra-fast speed using oriented hydrogel fibers. Adv Funct Mater 26(7):1021–1027
4. Formo E, Lee E, Campbell D, Xia Y (2008) Functionalization of electrospun TiO_2 nanofibers with Pt nanoparticles and nanowires for catalytic applications. Nano Lett 8(2):668–672
5. Xu WH, Ding YC, Jiang SH, Zhu J, Ye W, Shen YL, Hou HQ (2014) Mechanical flexible PI/MWCNTs nanocomposites with high dielectric permittivity by electrospinning. Europ Polym J 59:129–135
6. Xu WH, Ding YC, Jiang SH, Chen LL, Liao XJ, Hou HQ (2014) Polyimide/$BaTiO_3$/MWCNTs three-phase nanocomposites fabricated by electrospinning with enhanced dielectric properties. Mater Lett 135:158–161
7. Yang CR, Jia ZD, Guan ZC, Wang LM (2009) Polyvinylidene fluoride membrane by novel electrospinning system for separator of Li-ion batteries. J Power Sources 189(1):716–720
8. Ye W, Zhu J, Liao XJ, Jiang SH, Li YH, Fang H, Hou HQ (2015) Hierarchical three-dimensional micro/nano-architecture of polyaniline nanowires wrapped-on polyimide nanofibers for high performance lithium-ion battery separators. J Power Sources 299:417–424
9. Sill TJ, von Recum HA (2008) Electrospinning: applications in drug delivery and tissue engineering. Biomaterials 29(13):1989–2006
10. Sayed E, Karavasili C, Ruparelia K, Haj-Ahmad R, Charalambopoulou G, Steriotis T, Giasafaki D, Cox P, Singh N, Giassafaki LN, Mpenekou A, Markopoulou CK, Vizirianakis IS, Chang MW, Fatouros DG, Ahmad Z (2018) Electrosprayed mesoporous particles for improved aqueous solubility of a poorly water soluble anticancer agent: in vitro and ex vivo evaluation. J Control Release 278:142–155
11. Wu S, Li JS, Mai J, Chang MW (2018) Three-dimensional electrohydrodynamic printing and spinning of flexible composite structures for oral multidrug forms. ACS Appl Mater Interfaces 10(29):24876–24885
12. Wang BL, Ahmad Z, Huang J, Li JS, Chang MW (2018) Development of random and ordered composite fiber hybrid technologies for controlled release functions. Chem Eng J 343:379–389
13. Liu J, Yue Z, Fong H (2009) Continuous nanoscale carbon fibers with superior mechanical strength. Small 5(5):536–542
14. Huang ZM, Zhang YZ, Kotaki M, Ramakrishna S (2003) A review on polymer nanofibers by electrospinning and their applications in nanocomposites. Compos Sci Technol 63(15):2223–2253
15. Zhang CC, Gao CC, Chang MW, Ahmad Z, Li JS (2016) Continuous micron-scaled rope engineering using a rotating multi-nozzle electrospinning emitter. Appl Phys Lett 109(15):151903
16. Seidlits SK, Lee JY, Schmidt CE (2008) Nanostructured scaffolds for neural applications. Nanomedicine (London) 3(2):183–199
17. Liu X, Wei D, Zhong J, Ma M, Zhou J, Peng X, Ye Y, Sun G, He D (2015) Electrospun nanofibrous P(DLLA-CL) balloons as calcium phosphate cement filled containers for bone repair: in vitro and in vivo studies. ACS Appl Mater Interfaces 7(33):18540–18552
18. Sun G, Wei D, Liu X, Chen Y, Li M, He D, Zhong J (2013) Novel biodegradable electrospun nanofibrous P(DLLA-CL) balloons for the treatment of vertebral compression fractures. Nanomedicine 9(6):829–838
19. Duan GG, Jiang SH, Jerome V, Wendorff JH, Fathi A, Uhm J, Altstadt V, Herling M, Breu J, Freitag R, Agarwal S, Greiner A (2015) Ultralight, soft polymer sponges by self-assembly of short electrospun fibers in colloidal dispersions. Adv Funct Mater 25(19):2850–2856
20. Hsu PC, Wang S, Wu H, Narasimhan VK, Kong D, Ryoung Lee H, Cui Y (2013) Performance enhancement of metal nanowire transparent conducting electrodes by mesoscale metal wires. Nat Commun 4:2522
21. Wang XF, Ding B, Sun G, Wang MR, Yu JY (2013) Electrospinning/netting: a strategy for the fabrication of three-dimensional polymer nano-fiber/nets. Prog Mater Sci 58(8):1173–1243
22. Lee WS, Sunkara V, Han JR, Park YS, Cho YK (2015) Electrospun TiO_2 nanofiber integrated lab-on-a-disc for ultrasensitive protein detection from whole blood. Lab Chip 15(2):478–485
23. Sun B, Long YZ, Zhang HD, Li MM, Duvail JL, Jiang XY, Yin HL (2014) Advances in three-dimensional nanofibrous macrostructures via electrospinning. Prog Polym Sci 39(5):862–890
24. Jin G, Shin M, Kim SH, Lee H, Jang JH (2015) SpONGE: spontaneous organization of numerous-layer generation by electrospray. Angew Chem Int Ed Engl 54(26):7587–7591
25. Soliman S, Pagliari S, Rinaldi A, Forte G, Fiaccavento R, Pagliari F, Franzese O, Minieri M, Di Nardo P, Licoccia S, Traversa E (2010) Multiscale three-dimensional scaffolds for soft tissue engineering via multimodal electrospinning. Acta Biomater 6(4):1227–1237
26. Badrossamay MR, McIlwee HA, Goss JA, Parker KK (2010) Nanofiber assembly by rotary jet-spinning. Nano Lett 10(6):2257–2261
27. Zhang D, Chang J (2008) Electrospinning of three-dimensional nanofibrous tubes with controllable architectures. Nano Lett 8(10):3283–3287
28. Wang L, Ahmad Z, Huang J, Li JS, Chang MW (2017) Multicompartment centrifugal electrospinning based composite fibers. Chem Eng J 330:541–549
29. Paneva D, Manolova N, Rashkov I, Penchev H, Mihai M, Dragan ES (2010) Self-organization of fibers into yarns during electrospinning of polycation/polyanion polyelectrolyte pairs. Dig J Nanomater Bio 5(4):811–819
30. Frenot A, Henriksson MW, Walkenström P (2007) Electrospinning of cellulose-based nanofibers. J Appl Polym Sci 103(3):1473–1482
31. Wang BL, Zhou WY, Chang MW, Ahmad Z, Li JS (2017) Impact of substrate geometry on electrospun fiber deposition and alignment. J Appl Polym Sci 134(19):44823
32. Zhao S, Zhou Q, Long YZ, Sun GH, Zhang Y (2013) Nanofibrous patterns by direct electrospinning of nanofibers onto

topographically structured non-conductive substrates. Nanoscale 5(11):4993–5000
33. Zhang DM, Chang J (2007) Patterning of electrospun fibers using electroconductive templates. Adv Mater 19(21):3664
34. Yang H, Dong L (2009) Selective nanofiber deposition using a microfluidic confinement approach. Langmuir 26(3):1539–1543
35. Ding Z, Salim A, Ziaie B (2009) Selective nanofiber deposition through field-enhanced electrospinning. Langmuir 25(17):9648–9652
36. Shim IK, Suh WH, Lee SY, Lee SH, Heo SJ, Lee MC, Lee SJ (2009) Chitosan nano-/microfibrous double-layered membrane with rolled-up three-dimensional structures for chondrocyte cultivation. J Biomed Mater Res A 90(2):595–602
37. Shim IK, Jung MR, Kim KH, Seol YJ, Park YJ, Park WH, Lee SJ (2010) Novel three-dimensional scaffolds of poly(L-lactic acid) microfibers using electrospinning and mechanical expansion: fabrication and bone regeneration. J Biomed Mater Res B Appl Biomater 95(1):150–160
38. Wang W, Itoh S, Konno K, Kikkawa T, Ichinose S, Sakai K, Ohkuma T, Watabe K (2009) Effects of Schwann cell alignment along the oriented electrospun chitosan nanofibers on nerve regeneration. J Biomed Mater Res A 91(4):994–1005
39. Hull TC (2005) Origami design secrets: mathematical methods for an ancient art. Math Intell 27(2):92–95
40. Christian BA (1973) Principles that govern the folding of protein chains. Science 181(4096):223–230
41. Mahadevan L, Rica S (2005) Self-organized origami. Science 307(5716):1740
42. Andersen ES, Dong M, Nielsen MM, Jahn K, Subramani R, Mamdouh W, Golas MM, Sander B, Stark H, Oliveira CL (2009) Self-assembly of a nanoscale DNA box with a controllable lid. Nature 459(7243):73–76
43. Douglas SM, Dietz H, Liedl T, Högberg B, Graf F, Shih WM (2009) Self-assembly of DNA into nanoscale three-dimensional shapes. Nature 459(7245):414
44. Gracias DH, Kavthekar V, Love JC, Paul KE, Whitesides GM (2002) Fabrication of micrometer-scale, patterned polyhedra by self-assembly. Adv Mater 14(3):235
45. Leong TG, Randall CL, Benson BR, Bassik N, Stern GM, Gracias DH (2009) Tetherless thermobiochemically actuated microgrippers. Proc Natl Acad Sci USA 106(3):703–708
46. Bassik N, Stern GM, Jamal M, Gracias DH (2008) Patterning thin film mechanical properties to drive assembly of complex 3D structures. Adv Mater 20(24):4760–4764
47. Cho J-H, Gracias DH (2009) Self-assembly of lithographically patterned nanoparticles. Nano Lett 9(12):4049–4052
48. Guo X, Li H, Ahn BY, Duoss EB, Hsia KJ, Lewis JA, Nuzzo RG (2009) Two-and three-dimensional folding of thin film single-crystalline silicon for photovoltaic power applications. Proc Natl Acad Sci USA 106(48):20149–20154
49. Syms RR, Yeatman EM, Bright VM, Whitesides GM (2003) Surface tension-powered self-assembly of microstructures-the state-of-the-art. J Microelectromech Syst 12(4):387–417
50. Py C, Reverdy P, Doppler L, Bico J, Roman B, Baroud CN (2007) Capillary origami: spontaneous wrapping of a droplet with an elastic sheet. Phys Rev Lett 98(15):156103
51. Szczepanowicz K, Dronka-Gora D, Para G, Warszynski P (2010) Encapsulation of liquid cores by layer-by-layer adsorption of polyelectrolytes. J Microencapsul 27(3):198–204
52. Song J, Gao H, Zhu G, Cao X, Shi X, Wang Y (2015) The preparation and characterization of polycaprolactone/graphene oxide biocomposite nanofiber scaffolds and their application for directing cell behaviors. Carbon 95:1039–1050
53. Song J, Zhu G, Wang L, An G, Shi X, Wang Y (2017) Assembling of electrospun meshes into three-dimensional porous scaffolds for bone repair. Biofabrication 9(1):015–018
54. Okamoto M, Dohi Y, Ohgushi H, Shimaoka H, Ikeuchi M, Matsushima A, Yonemasu K, Hosoi H (2006) Influence of the porosity of hydroxyapatite ceramics on in vitro and in vivo bone formation by cultured rat bone marrow stromal cells. J Mater Sci Mater Med 17(4):327–336
55. Yang C-Y, Lee T-M, Yang C, Chen L, Wu M, Lui T (2007) In vitro and in vivo biological responses of plasma-sprayed hydroxyapatite coatings with posthydrothermal treatment. J Biomed Mater Res A 83(2):263–271
56. Meng Z, Zheng W, Li L, Zheng Y (2010) Fabrication and characterization of three-dimensional nanofiber membrance of PCL–MWCNTs by electrospinning. Mater Sci Eng C 30(7):1014–1021
57. Lee K, Kim H, Khil M, Ra Y, Lee D (2003) Characterization of nano-structured poly(ε-caprolactone) nonwoven mats via electrospinning. Polymer 44(4):1287–1294
58. Nojima S, Hashizume K, Rohadi A, Sasaki S (1997) Crystallization of ε-caprolactone blocks within a crosslinked microdomain structure of poly(ε-caprolactone)-block-polybutadiene. Polymer 38(11):2711–2718
59. Chen J-P, Chang Y-S (2011) Preparation and characterization of composite nanofibers of polycaprolactone and nanohydroxyapatite for osteogenic differentiation of mesenchymal stem cells. Colloid Surf B 86(1):169–175
60. Wan C, Chen B (2011) Poly (ε-caprolactone)/graphene oxide biocomposites: mechanical properties and bioactivity. Biomed Mater 6(5):055010
61. Arraiza AL, Sarasua J, Verdu J, Colin X (2007) Rheological behavior and modeling of thermal degradation of poly (ε-caprolactone) and poly(L-lactide). Int Polym Process 22(5):389–394
62. Ma H, Su W, Tai Z, Sun D, Yan X, Liu B, Xue Q (2012) Preparation and cytocompatibility of polylactic acid/hydroxyapatite/graphene oxide nanocomposite fibrous membrane. Chin Sci Bull 57(23):3051–3058